UNIVERSITY OF PETROLEUM AND ENERGY STUDIES

Aerodynamic performance study for a low Reynolds number aerofoil using micro vortex generators

by

Mohd Afeef Badri

Supervisor

Assistant professor Karthik Sundarraj

Department of Aerospace Engineering

Program: MTech CFD

05, April, 2014

Foreword

I would like to express my deep appreciation and thanks for my thesis supervisor **Mr. Karthik Sundarraj**, Assistant Professor Aerospace Department, UPES. Throughout the process of completing my thesis I obtained much help and encouragement from him.

I would also like to thank Professor **Dr. Ugur Guven**, course director M. Tech. CFD, Department of Aerospace Engineering, UPES, who has always been a source of inspiration for me.

I would like to pay my sincere thank to **Mr. Manoj Joishi**, **Mr. Geetesh Wagela**, **Mr. Anurag Singh** and all my batch mates for encouraging me and helping me with the project.

Finally I am in debt to my parents who were there supporting me all the times I need them.

Summary

This thesis highlights and reviews the use of micro vortex generators for boundary layer and flow separation control. Micro vortex generators (MVG's) or low profile vortex generators (VG's) find their application both in aerofoil/wing aerodynamic enhancement area and in non aerofoil/wing applications. This thesis only covers the aerofoil/wing application area of MVG's. Performance enhancement via MVG's is achieved by increasing the lift and reduction of drag in low Re aerofoils, high lift aerofoils, transonic aerofoil, and high swept wings. Most effective MVG for laminar flow region is called as "wishbone MVG" for which $h/\delta = 0.3$ and $\Delta z/\delta = 19$. A slotted Clark Y aerofoil geometry is analyzed in ANSYS (FLUENT) and design modification by adding different type of MVG's at different locations of the flap is tested for optimizing the aerodynamic performance of the flap hence increasing the lift of aerofoil. By careful placement of wishbone MVG's over the flap surface, a 25% increase in lift of the flap is obtained. Hence improving its performance. It is equally noted that, aerofoil total lift is increased by 13%. A FORTRAN code is developed to calculate the value of C_L for the flap using the C_p distribution and the value is compared against the values obtained by ANSYS (FLUENT).

Contents

Chapter 1

Introduction

For reduction of drag and improving the flow quality there is a need to reduce and/or control the boundary layer over the surface. Introducing vortex generators is one of the techniques to reduce the complications in flow caused due to boundary layer. Although other techniques such as flow vanes, boundary layer suction, laminar surfaces etc are available but introduction vortex generators is the most robust, easy in installation, light weighted, and simple of them all. Generally for aeronautical application the boundary layer is turbulent, and control of turbulent boundary layer is a huge topic in itself. There are many ways by which such boundary layer may be controlled. One such way is introduction of vortex generator which is the topic of this thesis.

Vortices formed in the boundary layer can help us to control the boundary layer, vortices inside the boundary layer can be formed using the micro vortex generators on the surface.

Micro vortex generators (MVG's) also called as low-profile or sub-profile boundary layer VG's are vortex generators having their height less than the boundary layer thickness of the surface. MVG's are known for improving the health of the flow or simply improving the flow conditions. Robustness and very less low profile drag are the obvious advantages of micro vortex generators. As the flow control involves formation of a micro vortex that is generated by the MVG there is no need of any actuating system making MVG's simpler and easy to implement. While MVG's might not produce as much changes in the flow field as is done by its other conventional counterparts, MVG's still are able to produce changes that are significant enough in improving the flow conditions and improving the capability of boundary layer to cope with the adverse pressure gradient. MVG's are best effective at low speeds as is shown by the past research being done on them.

Micro vortex generators operate the same ways as a conventional vortex generator does, i.e., it energizes the boundary layer by formation of vortices, although the clarity as to how the process exactly happens is still unknown. In simple words introducing swirling motion provides extra energy to the boundary layer needed by it to delay separation caused due to adverse pressure gradient.

There are studies being conducted which propose that MVG's can help to overcome the adverse effect caused due to boundary layer and shock interaction, the study is being carried out in both transonic and subsonic flow regimes. Large scale separation region is caused due to shock-wave boundary-layer interaction that causes low quality flow resulting in localize peak in heating and pressure can be controlled using MVG's, these high speed studies are conducted on MVG's for research purpose.

1.1 Purpose of the thesis

This thesis concentrates on aerodynamic implementation of MVG's to enhance performance of high lift device (slot) on a multi-element aerofoil. Lift can be improved in a wing by adding a flap (high lift device) to it, having a slotted flap enhances the lift more than having only flap. Hence by providing a flap it is possible to have more lift at same incidence and lower velocities, which enhances aircrafts performance while takeoff and landing.

For takeoff high values of C_L are required which are not met by the normal aerofoil (fig. 1.1a) hence there is a need to introduce flaps (fig. 1.1b) in some cases the values are not even met by introducing flaps alone hence there is a need to have slotted flap, or in some cases a slat or leading edge flap (fig. 1.1c). Usually with a single flaps it is difficult to produce considerable increase in $\max(C_L)$ mainly due to turbulent separation, this problem may be solved using multi-slot/multi-element aerofoils.

The use of vortex generators is widely employed in aeronautical engineering to rescue turbulent separation hence reducing pressure drag caused by it. The purpose of this thesis is to optimize the location of the MVG on the flap surface so that there is a delay in separation and $\max(C_L)$ of the aerofoil can be increased owing to the reduction in adverse pressure gradient on the trailing edge.

1.2 Background

Taylor back in 1947 [1] was the first to study the effect of vortex generators over the wing and how it affects the aerodynamic performance of the wing. Passive vortex generators which is the topic of this study were first developed by in [1], these were used to delay the boundary layer separation in wind tunnel diffuser. Systematically vortex generators and what effect they have on boundary layer were studied in detail by Schubauer and Spangenberg back in 1960 [2]. The conventional passive vortex generator was then being studied extensively. However, in 1994 Storms and Jang [3] suggested that vortex generators are not advisable for cursing speed as it involves increment in parasite drag. Also it is not easy to place a vortex generator in a slotted flap due to lack of space between the main aerofoil and the flap element. Hence, MVG's – due to their small size – are a good choice to apply in the case of a multi-element aerofoil. Novel trailing edge

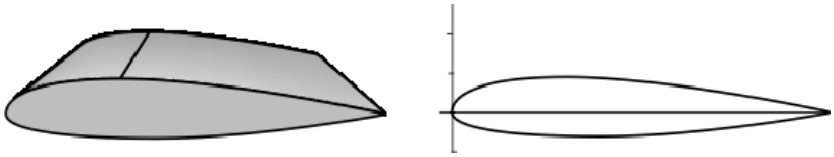

(a) simple wing and an aerofoil.

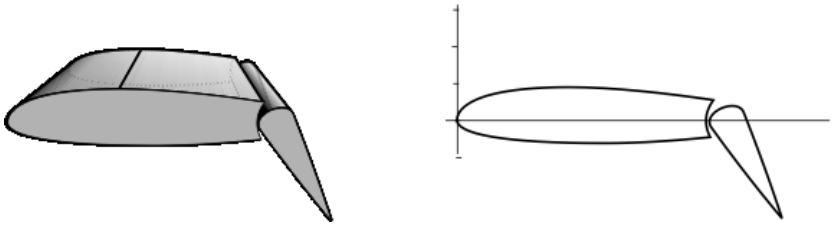

(b) a wing and an aerofoil with flap.

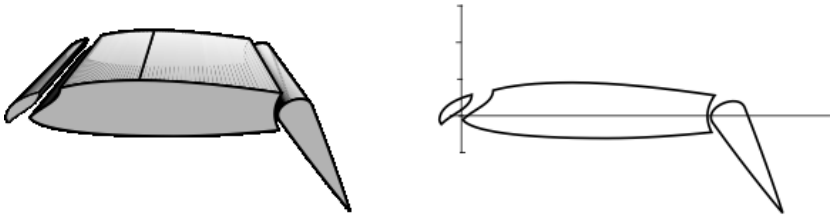

(c) a wing and an aerofoil with slot and flap.

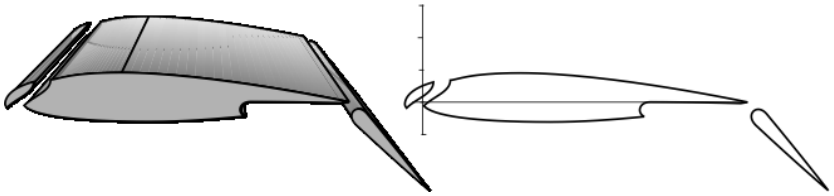

(d) a wing and an aerofoil with leading-edge slat and trailing-edge flap.

Figure 1.1: use of slots, slats, and flaps.

devices have been proposed by Werle et al. in 1987 [4] which helped in delaying the separation of the flow, these consists of waving the trailing edge in order to promote mixing of lower surface and upper surface flow to enhance lift. But waving of flap wing has a problem that it would make flap stowing impossible hence MVG's prove to be a good option for the wing with flaps.

In general, vortex generators are of two type active vortex generators and passive vortex generators [5]. Passive vortex generators are ones having fixed size, shape, positioning over and orientation over the flow wetted surface. Such MVG's have a narrow operational range. An in depth review of Passive type of MVG's was given by Lin JC [6], this work concentrated how passive MVG's help in controlling the boundary layer flow separation. Gordard et al. [7] conducted experiments to find the optimized location passive vane type VG's for delaying boundary layer separation. Two type of VG configurations were tested one producing a co and other counter rotating Vortices, and it was proven that the counter rotating vortex created appeared to be more effective in the case. The Active vortex generators are capable changing their size position, orientation and size according to the flow condition available. Shizawa and Mizusaki [8] studied active VG's effect over flat plate boundary layer. There are other evidences available that prove that active VG's energises the boundary layer and also enhances momentum mixing hence making it superior over passive VG's.

1.3 Hypothesis

For low Re number, flow over the aerofoil remains laminar. As laminar flows offer less resistance to adverse pressure gradient, these are more susceptible to flow separation. The separated shear layer is characterized by formation of vortices due to Kevin–Helmholtz mechanism. The present work propose is to find the optimal location of a low profile passive MVG by the use of CFD so that aerodynamics performance of the wing may be improved. MVG's produce a micro vortex that helps energising the flow, hence delaying the separation. This delayed separation would consequently enhance the lift of the aerofoil, and thereby enhancing its aerodynamic performance.

Chapter 2

Enhancing aerodynamic performance by application of vortex generators

In broader sense as to how MVG's help in delay of flow separation the area of research may be divided into two. First being the investigation of flow separation control application, and how it behaves for different aerofoil and wing configuration. Second is investigation of non aerofoil applications of MVG's through flow control. The details of research and investigations that are carried out on MVG's are presented in fig. 2.1, the table summaries the importance of parameters that are used for separation control in the flow, these include VG type, h/d, e/h, $\Delta z/h$, β, and VG location.

The study over aerofoil or a wing may be sub-categorized as: low Re aerofoil, aerofoil with high lifting devices, highly swept wing and transonic aerofoil/wings as shown in fig. 2.1. In depth discussion of the topic is present in sections 2.1 to 2.4. The non aerofoil/wing application study of MVG's may be sub categorized as: noise reduction using VG's, reducing inlet distortion in the engines these are shown in fig. 2.1 detailed discussion over such application will not be presented as it is beyond the scope of the thesis presented. The discussion in general covers the nature of flow separation and the phenomena associated with it also it goes on to provide proof of benefits that can be gained by the use of MVG's for these cases.

2.1 Aerofoil/wing applications at low Reynolds number

Many of the modern aerofoils have the capabilities to operate for a low range of Reynolds number, such aerofoils find its application in unmanned air vehicles, high altitude long endurance aircraft wings, wind turbine blades, and compressor blades. Typical chord Re rage of operation for such aerofoils is below one million hence such flows fall in laminar flow regime and often such flows ex-

Investigator(s) (year pub.)	Test bed	Type of study	Flow parameters	Most effective VG parameters examined						Comments
				VG type	h	e/h	$\Delta z/h$	β (deg)	VG placement	
Noise reduction for Gulfstream III										
Holmes et al. (1987)	Gulfstream III aircraft	Flight test	$M_\infty = 0.78$ to 0.85, $\delta \sim 1$ in	Counter-rotating rectangular vanes	$1/8\delta$	8	18	± 30	122 in from the aircraft nose (up to about $50h$ up-stream of the shock location)	Up to 5 dB interior noise reduction via delayed shock-induced separation and attenuated Kármán vortex street shed from canopy shock wave.
Engine face distortion management in compact inlets:										
Anabtawi et al. (1999)	Diffusing S-duct	Wind-tunnel test	$M_\infty = 0.05$, $Re_d = 0.5 \times 10^6$	Co-rotating rectangular vanes	0.25δ 0.5δ	10 3	~ 4 ~ 3	~ 16 ~ 16	VG LE at the duct throat	Non-optimum VG placement and small number of device caused the low-profile VGs to be less effective than conventional VGs.
Anderson et al. (1999)	DERA/M2129 inlet S-duct	CFD and DOE	$M_{th} = 0.794$, $Re = 16 \times 10^6$ per feet	Co-rotating rectangular vanes	$\sim \theta$, 2–4 mm	12	~ 12	24	2 throat radius from the inlet	Attenuate large pair of baseline counter-rotating vortices resulting in reduction of DC(60) engine face distortion by over a factor of 3. A reduced CFD model eliminates the need to model the VG geometry.
Hamstra et al. (2000)	4:1 aspect ratio ultra-compact serpentine duct	Wind-tunnel Test	$M_{th} = 0.43$ to 0.68, $Re_d = 3 \times 10^6$	Co-rotating rectangular vanes	$\sim \theta$, 2–3 mm	12	~ 12	24	2 stations down-stream of inlet throat	Up to 5% increase in total pressure recovery. Up to 50% decrease in DC(60) spatial distortion and RMS turbulence.
Overwing fairing of V-22:										
Tai (2002)	V-22 overwing fairing	CFD	$M_\infty = 0.345$	Counter-rotating trapezoidal vanes	0.5δ	3	~ 3	± 9	$\sim 10h$ upstream of baseline separation	New gridding method allows VGs incorporated onto full aircraft for CFD design analysis. Mild separation and marginal benefit predicted for VGs using Baldwin–Lomax turbulence model.

Investigator(s)	Test bed	Type of study	Flow parameters	Most effective VG parameters examined						Comments
				VG type	h	e/h	$\Delta z/h$	β (deg)	VG placement	
Low-Reynolds number airfoil:										
Kerho et al. (1993)	Liebeck LA2573A low-Re airfoil	Wind-tunnel test	$Re_c = 20{,}000$ to 500,000, $\delta = 1.6$ mm	Wishbones	0.3δ	10	65	± 27	22% airfoil chord (just up-stream of laminar separation bubble)	0.48-mm-high wishbone VGs can produce a desirable eddy structure without prematurely produce turbulent boundary layer resulting in 38% drag reduction.
				Ramp cone	0.4δ	9	40	60		
High-lift airfoils:										
Lin et al. (1994) Lin (1999)	3-element high-lift airfoil	Wind-tunnel test	$M_\infty = 0.2$, $Re_c = 5$ and 9×10^6	Counter-rotating trapezoidal vanes	0.2δ	7	13	± 23	25% flap chord (30 h upstream of separation on flap)	0.04-in-high VGs produced 10% lift increase, 50% drag reduction, and 100% increase in L/D. VGs allow stowage inside the flap well during aircraft cruise.
Klausmeyer et al. (1996)	3-element high-lift airfoil	Wind-tunnel test	$U_\infty = 140$ ft/s	Counter-rotating, trapezoidal vanes	0.2δ	7	13	± 23	20% flap chord (27 h upstream of separation on flap)	0.04-in-high VGs produced streamwise vortices strong enough to control separation without dominating the flow field afterward.
Highly swept wings:										
Ashill et al. (1994)	60° LE delta wing model	Wind-tunnel test	$M_\infty = 0.18$, $Re_c = 4 \times 10^6$	Co-rotating wires	$\sim\theta$	45	~ 87	~ 14	50 h from wing LE	0.51-mm-dia. wire VGs provided up to 16% reduction in K and delayed the onset of buffet by 10% in C_L.
Ashill et al. (1994)										
Ashill et al. (1995)										
Ashill et al. (1998)										
Langan and Samuels (1995)	40° LE diamond wing model	Wind-tunnel test	$M_\infty = 0.19$, $Re = 4 \times 10^6$/m $\delta = 0.1$ in	Co-rotating vanes	0.5δ	4	12	30	Wing tip Forward/outboard	0.05-in-high co-rotating VGs provided up to 5% increase in max. L/D.
					0.5δ	4	9	10		
Transonic airfoil:										
Ashill et al. (2001)	RAE 5243 transonic airfoil	Wind-tunnel test	$M_\infty = 0.67$ to 0.71, $Re_c = 19 \times 10^6$	Counter-rotating vanes	$\sim\delta^*$	~ 10	12	± 14	70 h upstream of shock location	0.76-mm-high vanes spaced 1 h apart produced over 20% increase in maximum lift. Forwards wedges increased maximum L/D by 5%.
				Forward wedges	$\sim\delta^*$	10	12	± 14		

Figure 2.1: Summary of research aerofoil/wing aerodynamic performance enhanced by MVG's.

perience a laminar separation bubble for low angles of attack generally below stall region. Generally, the separation bubble is formed near the boundary layer separation area the reason being maximum suction pressure or adverse pressure gradient is available in such area, this results in an unstable shear layer near to the surface that rapidly transits to a reattached turbulent boundary layer. Small separation bubbles have almost neglecting effect on C_L of aerofoil although it heavily affects C_D of the aerofoil hence reducing aerodynamic efficiency. If the separation bubble can be controlled or reduced that would result in a thinner turbulent boundary layer hence increasing the aerofoils performance. This is one of the application areas of MVG's, i.e., to reduce the thickness of turbulent boundary layer in such aerofoils.

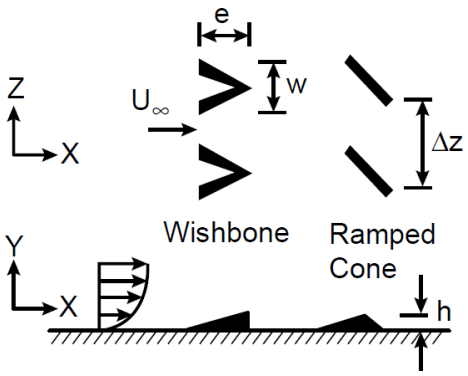

Figure 2.2: Wishbone MVG and ramped cone MVG [9].

Kerho et al. [9] presented experimental work on a low Re aerofoil (Liebek LA2573A), authors tried to reduce the separation bubble in the aerofoil by using MVG's and thereby reduced C_D. The Re range of the aerofoil was between 2 million to 5 million, which is a typical range of low Reynolds number aerofoil. MVG's produce micro vortices at the VG's trailing edge energizing the flow to overcome the adverse pressure gradient, and hence suppressing the separation bubble. Wishbone MVG's with $h/\delta = 0.3$, ($\delta = 1.6$ mm) and ramp cone MVG's with $h/\delta = 0.4$ are two different types of MVG's fig. 2.2 that are tested. The results can be seen in fig. 2.3.

2.2 High lift aerofoil

High lift aerofoils are the most frequently used ones in commercial transport aircrafts. There is more flow separation in a multi-element aerofoil (fig. 2.4) than compared to a simple one as it is a function of complicated geometry of the aerofoil and the flying conditions. For such cases boundary layer separation is exhibited by the aerofoil at much lower angles of attack than the conventional aerofoil. Altering the geometry for avoiding such conditions would not be a good option as it may complicate the geometry even further hence MVG's find a good application in this field of aeronautics.

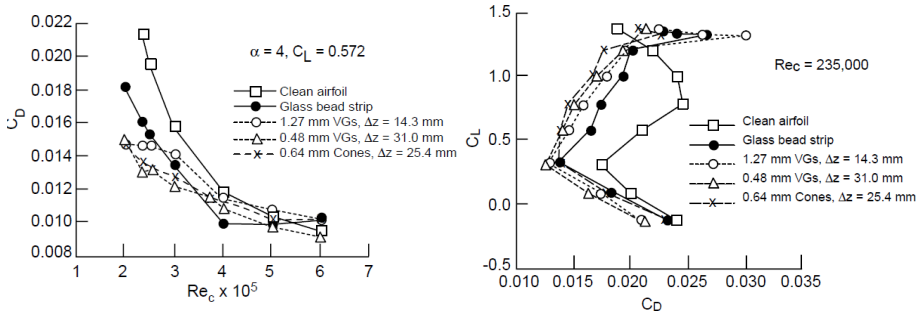

(a) C_D vs. Re for a low Re aerofoil with MVG's.

(b) C_L vs. C_D for a low Re aerofoil with MVG's.

Figure 2.3: Performance curves for VG's [9].

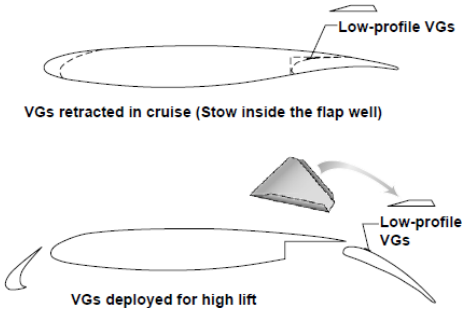

Figure 2.4: multi-element aerofoil with a MVG [10].

NASA in early 1990s conducted research on high lift performance enhancement using MVG's [10]. The tests were conducted on a single flap three element aerofoil and results are presented in fig. 2.5. Tests were conducted on Reynolds number ranging from 5 to 9×10^6 these Reynolds number represent the cursing condition Reynolds number for a commercial airplane.

As can be seen by fig. 2.5, placing the MVG over the flap surface enhances the pressure distribution over the aerofoil thus resulting in better lift distribution hence more C_L. A active MVG, counter rotating, trapezoidal wing MVG with ($h/c = 0.0018$, $e/h = 7$, $\beta = 23°$) located at $0.25C$ is used for the study presented.

2.3 High swept wings

Ashille et al. [12] used minute wire segments as MVG's to control leading edge flow separation on high sweep back wing. these are referred to as "swept back vortex generators" (SBVG's). Such MVG's are suitable for wings with sweep angle greater than 40°. Such devices increase the maneuvering ability of aircraft by reducing the induced drag at subsonic speeds.

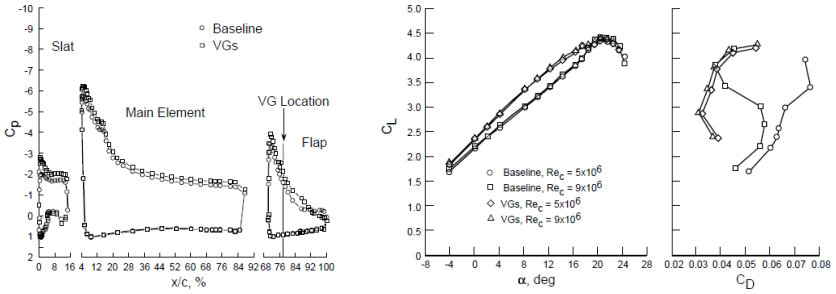

(a) pressure distibution. (b) C_L vs. α and C_L vs. C_D.

Figure 2.5: effect of MVG on multi-element aerofoil at $M = 0.2$. For C_p plot in (a) $\alpha = 8°, Re = 9 \times 10^6$ [11].

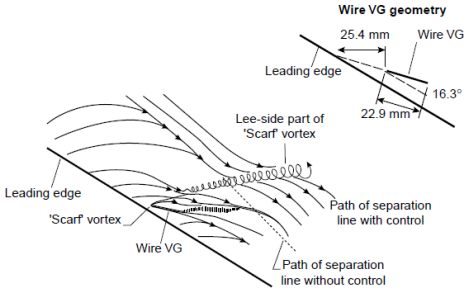

Figure 2.6: wire type VG over the wing surface [13].

MVG's in this case are small wires fig. 2.6 with $d = 0.51$ mm and $e/d = 45$, approximately equal to δ^*. Each wire is arranged in a sense so that it produces a stream-wise vortex, the rotation of the vortex is such that it resists the drift of boundary layer flow. Oil flow studies prove that the wires help in converting the boundary layer vortices to stream-wise vortices hence reducing the induced drag. Experimentally it is said to do so by producing a scarf vortex that is nothing but the stream-wise vortex created by the wire.

These kind of MVG's are used with modern fighter aircrafts enhancing their maneuver performance. As during combat the advanced fighter jets are required to have aggressive and high maneuver capabilities, such things are characterized by vortices in flow field and highly separated flow over wings. Such kind of flow fields lead in reduction of effectiveness of aerodynamics control. Implementing MVG's enhances the flow health hence giving better aerodynamic control over the jet. A fighter using MVG's is shown in fig. 2.7.

2.4 Transonic aerofoil

An aircraft during transonic flight operations encounters very large adverse pressure gradient due to boundary layer separation due to shock waves being formed in the transonic region. Separation may lead to loss of lift and loss of control

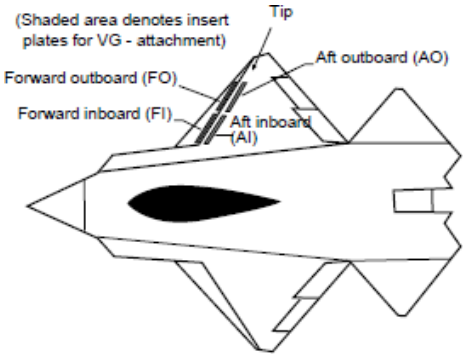

Figure 2.7: fighter aircraft implementing MVG's [14].

over the aircraft, higher drag and buffeting. A possible solution for such case is the use of low profile VG with the aerofoil to delay the separation [15].

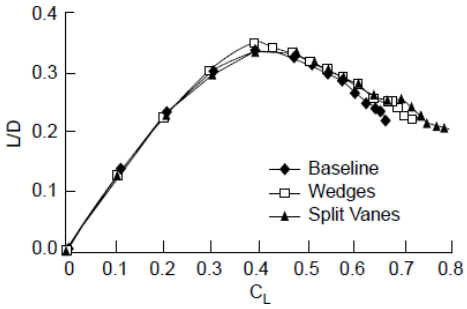

Figure 2.8: effect of MVG on L/D for a transonic aerofoil ($M = 0.71$) [12].

Ashill et al. [16] tested RAE 5243 aerofoil under transonic conditions and proved that lift can be enhanced if MVG's were used with the aerofoil the results can be seen in fig. 2.8. He used SBVG's type of vortex generator located at 55% of the cord and obtained almost 10% increase in lift.

Chapter 3

CFD analysis

3.1 CFD over a low profile MVG for a low Re aerofoil

CFD analysis on a low Re multi-element aerofoil Clark Y is performed to find out the optimized location of MVG for enhancing its aerodynamic performance. The reason for choosing Clark Y is that such aerofoil performs good under low speed and low Reynolds number conditions. As we are dealing with a low Re for the flow it will be assumed to remain laminar.

3.2 Governing equations

The flow here is being treated as a 2D flow. It is then governed by a two-dimensional Navier–Stokes equation fo a compressible flow in generalized curvilinear coordinates (ξ, η) the equation is given by

$$\frac{1}{J}\frac{\partial Q}{\partial t} + \frac{\partial \left(E + E_v\right)}{\partial \xi} = 0 \tag{3.1}$$

The invicid flux vectors E and F, the viscous flux vectors E_v and F_v and the conserved vector Q are given as:

$$Q = \begin{pmatrix} \rho \\ \rho u \\ \rho v \\ E_t \end{pmatrix}, \quad \mathrm{E} = \frac{1}{J}\begin{pmatrix} \rho U \\ \rho U u + p\xi_x \\ \rho U v + p\xi_y \\ U\left(E_t + p\right) \end{pmatrix}, \quad \mathrm{F} = \frac{1}{J}\begin{pmatrix} \rho V \\ \rho V u + p\eta_x \\ \rho V v + p\eta_y \\ V\left(E_t + p\right) \end{pmatrix}, \tag{3.2}$$

$$E_v = \frac{1}{J}\begin{pmatrix} 0 \\ \tau_{xx}\xi_x + \tau_{yx}\xi_y \\ \tau_{xy}\xi_x + \tau_{yy}\xi_y \\ Q_x\xi_x + Q_x\xi_y \end{pmatrix}, \quad \text{and} \quad F_v = \frac{1}{J}\begin{pmatrix} 0 \\ \tau_{xx}\eta_x + \tau_{yx}\eta_y \\ \tau_{xy}\eta_x + \tau_{yy}\eta_y \\ Q_x\eta_x + Q_x\eta_y \end{pmatrix} \tag{3.3}$$

where $J = \partial(\xi, \eta)/\partial(x, y)$ is the Jacobian for the coordinate transformation. The curvilinear coordinated are given by (ξ, η) and the Cartesian are given by (x, y), ξ_x, ξ_y, η_x, η_y are the metric terms for the transformation. u and v are

the velocities in x and y direction ρ is the density. E_t is the total energy given by:

$$E_t = \frac{p}{\gamma - 1} + \frac{1}{2}\rho\left(u^2 + v^2\right) \tag{3.4}$$

The covarient velocity components of U and V are given as:

$$\begin{aligned} \mathrm{U} &= u\xi_x + v\xi_y \\ \mathrm{V} &= u\eta_x + v\eta_y \end{aligned} \tag{3.5}$$

The Q_x and Q_y terms in the energy equations are given as:

$$\begin{aligned} \mathrm{Q}_x &= -q_x + u\tau_{xx} + v\tau_{xy} \\ \mathrm{Q}_y &= -q_y + u\tau_{yx} + v\tau_{yy} \end{aligned} \tag{3.6}$$

q_x and q_y are the heat fluxes in x and y directions respectively and τ_{xx}, τ_{yy}, τ_{yx}, and τ_{xy} are the viscous shear stresses. Mach number M, Reynolds number Re, Prandtl number Pr, and specific heat ratio γ are defined as:

$$M = \frac{U}{\sqrt{\gamma RT}}; \quad Re = \frac{\rho UL}{\mu}; \quad Pr = \frac{C_p}{\mu k}; \quad \gamma = \frac{C_p}{C_v} \tag{3.7}$$

R is the gas constant C_p and C_v are the specific heats at constant pressure and constant volume. Viscosity is determined according to Sutherland's law in dimensionless form given by

$$\mu = \frac{T^{\frac{3}{2}}(1+S)}{T+S} \text{ and } S = \frac{110.3\ K}{T_\infty} \tag{3.8}$$

The governing equation of state is giving by

$$\gamma M^2 p = \rho T \tag{3.9}$$

The components of viscous stress tensor and the heat fluxes in the non dimensional form is give by

$$\begin{aligned} \tau_{ij} &= \frac{\mu}{Re}\left[\left(\frac{\partial u_i}{\partial x_j}\right) + \left(\frac{\partial u_j}{\partial x_i}\right) - \frac{2}{3}\delta_{ij}\frac{\partial u_k}{\partial x_k}\right] \\ q_i &= -\frac{\mu}{(\gamma-1)M^2 RePr}\frac{\partial T}{\partial x_i} \end{aligned} \tag{3.10}$$

For in depth explanation of these governing equations please refer [17, 18].

3.3 Geometric modeling

Single slotted Clark Y geometry was constructed using ICEM CFD (ANSYS).

Clark Y aerofoil coordinate points are given in appendix A.1, these coordinates were imported into ICEM CFD as a point coordinate file and aerofoil was constructed. For the aerofoil flap and the slot it was cut out using fig. 3.1 as reference. Aerofoil chord length of 1 m was chosen for the study. The design parameters are given in the table table 3.1.

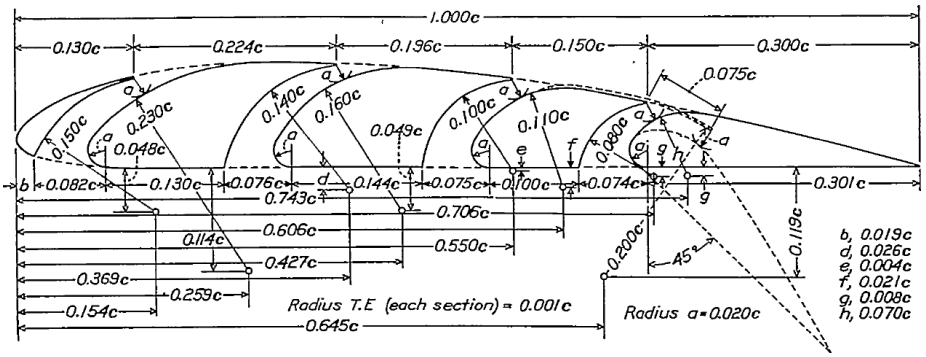

Figure 3.1: Clark Y aerofoil geometry with slat slot locations [19].

Table 3.1: Clark Y aerofoil Design parameters.

Description	Dimension (m)
Chord length (C)	1.000
Flap chord (Cf)	0.301
Trailing Edge (Rt)	0.001
Leading Edge (Rl)	0.020

Using table 3.1 as reference the Slotted flap multi-element Clark Y aerofoil as was constructed in ICEM CFD the same can be seen in fig. 3.2.

Figure 3.2 shows the Clark Y aerofoil model which was created using spline function in ICEM geometry creation module by joining all the points that where imported from appendix A.1. After creating the aerofoil the domain was wrapped around the model. C topology for domain was chosen with 12.5 chord length above below and ahead of the aerofoil and 20 chord length behind the aerofoil as can be seen in fig. 3.3.

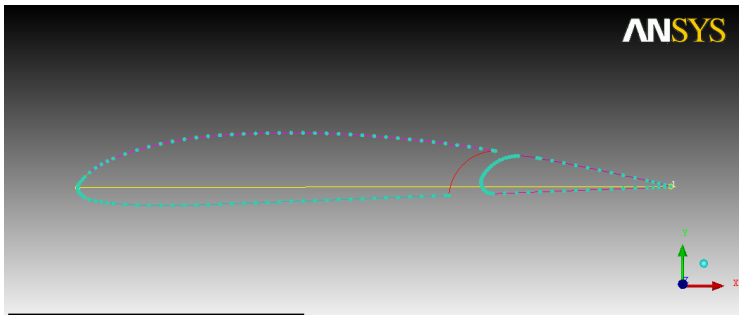

Figure 3.2: Clark Y aerofoil modeled in ICEM CFD.

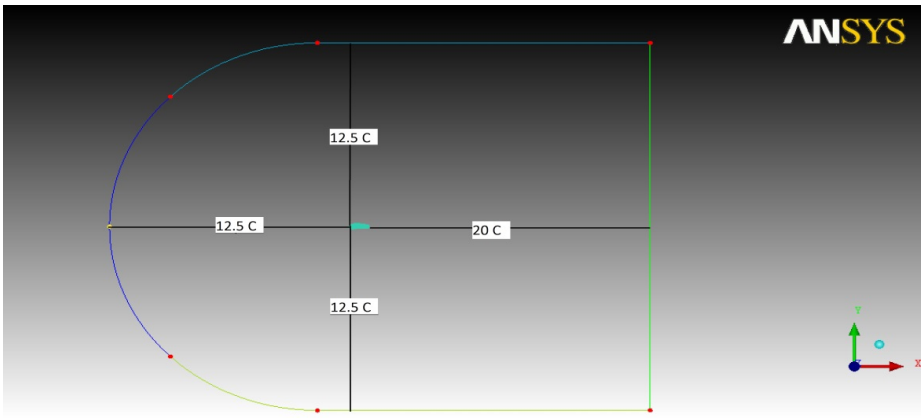

Figure 3.3: fluid domain around aerofoil.

3.4 Domain description: zones and parts

Zones and parts need to be created after the modeling part is over, as on these zones and parts during solving the boundary conditions and operational conditions are applied. Zones define the operational region of the domain and the boundaries are the enclosing geometries of the zones. In general zones and parts may be divided into two classes:

- Boundary type.
- Continuum type.

Boundary type includes the external and the internal boundaries of the domain, these are defined by points in 1D problems, lines in 2D problems and surfaces in 3D problems. Some of the common boundary types are wall, outlet, inlet, vent etc.

Continuum type includes the area of the domain which has a phase continuum i.e., it is solid or a fluid etc. Some available zone types are pressure inlet, pressure outlet, pressure farfield, porous medium, moving boundary, mass flow inlet, inlet, outlet, vent, inflow,surface,symmetry, velocity inlet, velocity outlet etc.

The zones and the parts for the model are shown in fig. 3.4 and are described in table 3.2.

As shown by the table the model has total of 5 parts and one zone. Main aerofoil is divided into two parts 'main element' and 'flap' these form the wall of the aerofoil. The interior of the domain is considered to be continuum type of zone containing air.

3.5 Meshing

ICEM CFD (ANSYS) was chosen for meshing the domain. The reason for choosing ICEM CFD's (ANSYS) meshing tool for the task is that its mesh

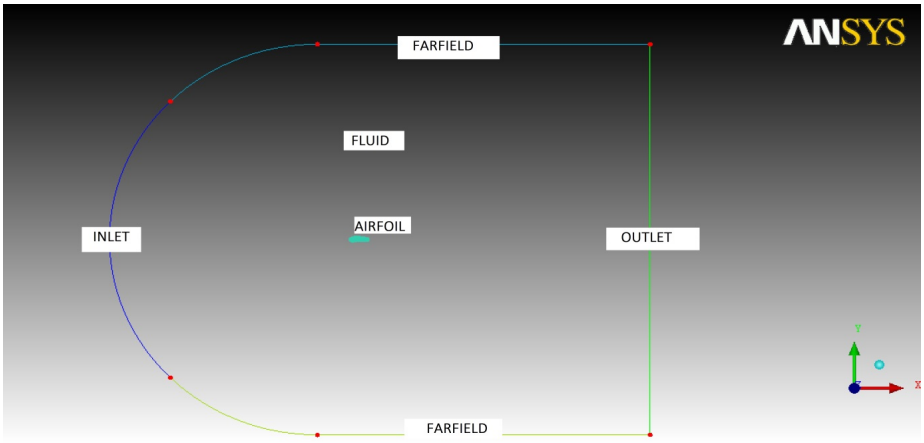

Figure 3.4: computational domain showing parts and zones.

Table 3.2: parts and zones of the domain.

Entity	Type
fluid	
Inlet boundary	velocity inlet
Outlet boundary	pressure outlet
Farfield boundary	no shear wall
Fluid zone	air
aerofoil	
Main element boundary	no slip wall
Flap boundary	no slip wall

generation tool is capable of parametrically mesh the model in may formats:

- Multiblock Structured meshing
- Unstructured hexahedral meshing
- Unstructured tetrahedral meshing
- Cartesian mesh with H-grid refinement
- Hybrid meshing
- Quad and triangular surface meshing

A multiblock structured meshing strategy was chosen to mesh the domain. The blocking strategy involved an O-grid on the periphery of the C-grid and multiblocks near the aerofoil as can be seen in fig. 3.5. A multiblocked meshes provide the users to have better control over the mesh parameters.

As can be seen in the figure the outer blocks 9 to 12 are a part of O-grid outer block and the inner core is further blocked to give a dense mesh near the surface of the aerofoil. Structured mesh quality of about 80% was obtained with total elements: 159,825 and total nodes: 158,985.

Figure 3.6 we can notice a denser mesh at the walls of the aerofoil as denser mesh is needed to capture the boundary layer properly. $Y+$ value of 1×10^{-4} is used with the mesh, also as can be seen in the fig. 3.6 high density mesh is developed in between the slot to capture effects that occurring in the slot.

Given fig. 3.7 shows the total mesh that was developed for the analysis the parameters are of mesh are depicted in the table 3.3.

Table 3.3: Mesh parameters.

Parameter	Value
Total nodes	159825
Total element	158985
Total faces	228624
Total blocks	7
Mesh quality	80%

3.6 Boundary conditions

Table 3.4 gives the summary of the boundary conditions used for the model. Air is assumed to flow in through the inlet at standard temperature and pressure (STP) with density ρ of 1.225 kg/m^3 and viscosity μ of 1.7894 $\times 10^{-5}$ inlet (part) is chosen to be the velocity inlet and Air is assumed flows in through inlet at a velocity of 55 m/sec. As the inlet is curved air is flown in the x direction i.e., normal to the inlet.

At outlet we assume the air to get back to STP condition hence the outlet is chosen as pressure outlet with a pressure of 101,325. For the farfields zero

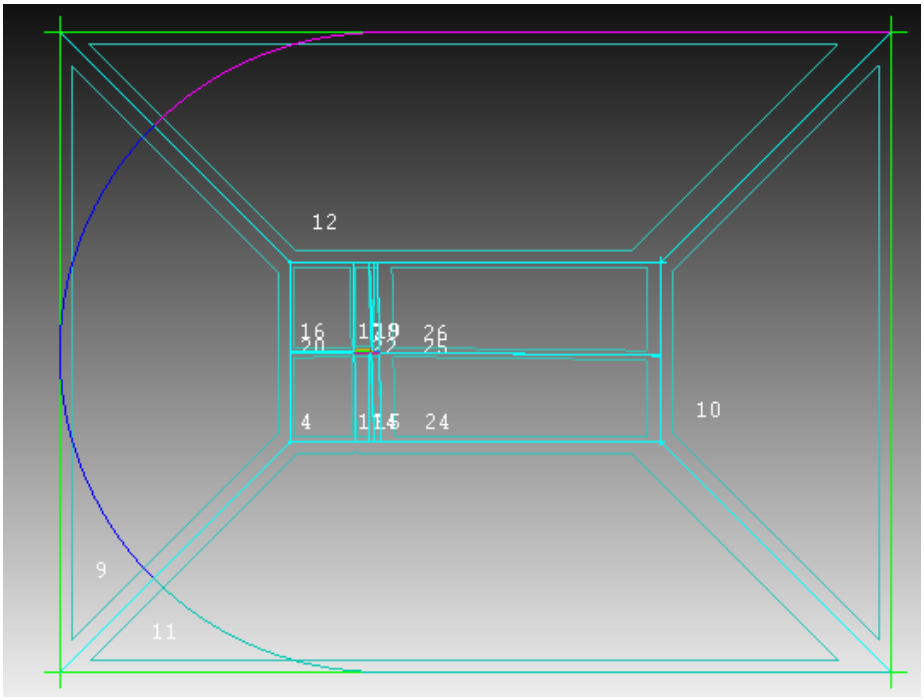

(a) full computational domain.

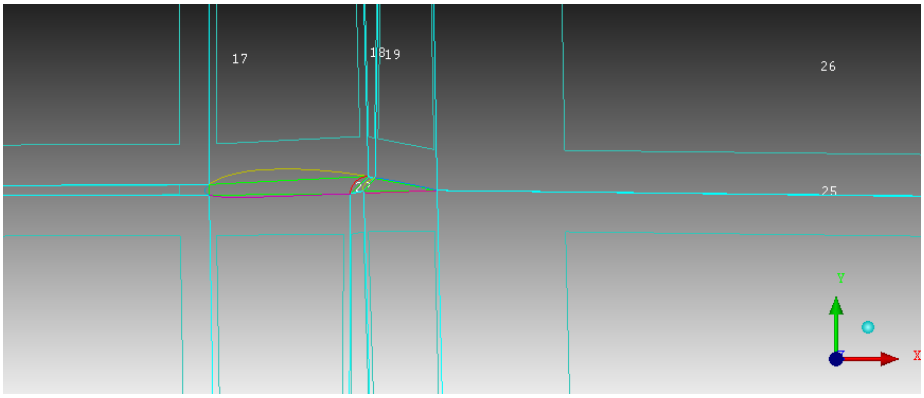

(b) zoom section around aerofoil.

Figure 3.5: blocking strategy for meshing the aerofoil.

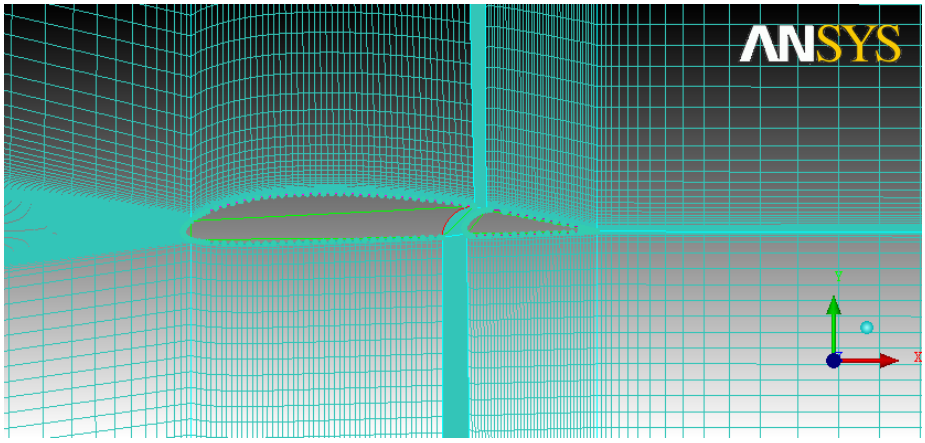

Figure 3.6: zoom of meshed Clark Y aerofoil.

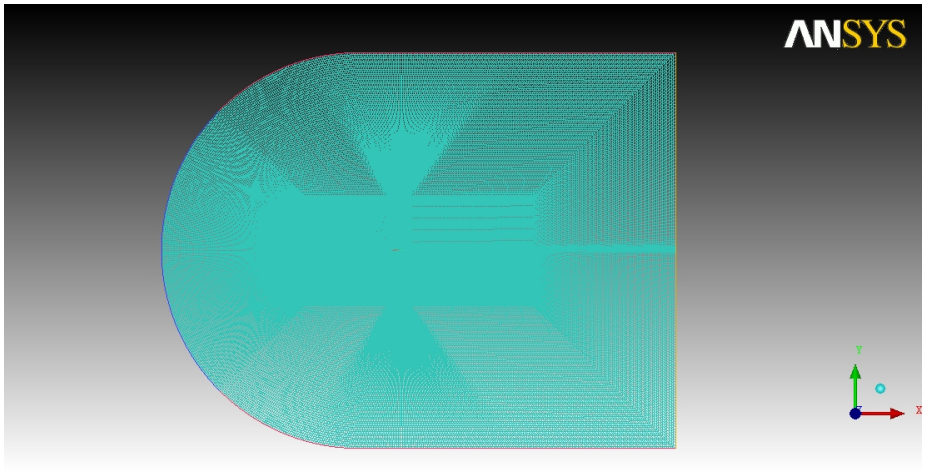

Figure 3.7: C-grid meshing over aerofoil.

Table 3.4: Boundary conditions.

Part/Zone	Boundary condition
Inlet	*Velocity inlet*
	Velocity magnitude = 55 m/s
	Velocity direction = x-axis
Outlet	*pressure outlet*
	Gauge pressure= 0 atm
	Backflow direction = normal to boundary
Aerofoil main Element	*Wall*
	Stationary no slip wall
	Roughness 0.5
Aerofoil flap	*Wall*
	Stationary no slip wall
	Roughness 0.5
Farfield	*Wall*
	Stationary wall with zero shear
Fluid	*interior*

shear stationary wall is assumed as the flow is assumed to return its original velocity and conditions as it reaches the farfield. Aerofoil is split into two parts the main element and the flap both are assumed to be no slip shear walls with a roughness factor of 0.5. As out flow is laminar and much of the work depends on boundary layer capturing hence no lip condition is assumed.

3.7 Solver model and initial condition

ANSYS FLUENT was used for solving the problem, 2D double precision serial processing was used. Inlet velocity as can be seen from the boundary condition section is assumed to be 55 m/sec this makes the flow incompressible as M is approximately 0.15 for such flow also for such flow with low velocity and such mach number the chordal Reynolds number is 300,000 which makes the flow laminar. Laminar flow model pressure based is used for solving the problem. Energy equation is not turned on as thermodynamic changes are assumed to be neglected.

Standard initialization strategy is used and the solution is initialized used inlet values i.e., zero gauge pressure and 55 m/sec velocity. Second order discretization scheme is used for pressure and momentum under SIMPLEC solving strategy and the convergence criteria is chosen to be 1×10^{-5} for time constrain. Skewness correction of 4 is used with SIMPLEC solver.

3.8 Results and discussions

Using the above boundary conditions and the solver conditions multi-element aerofoil with clean geometry was analyzed and results were observed. Figure 3.8 shows the pressure contours of the aerofoil.

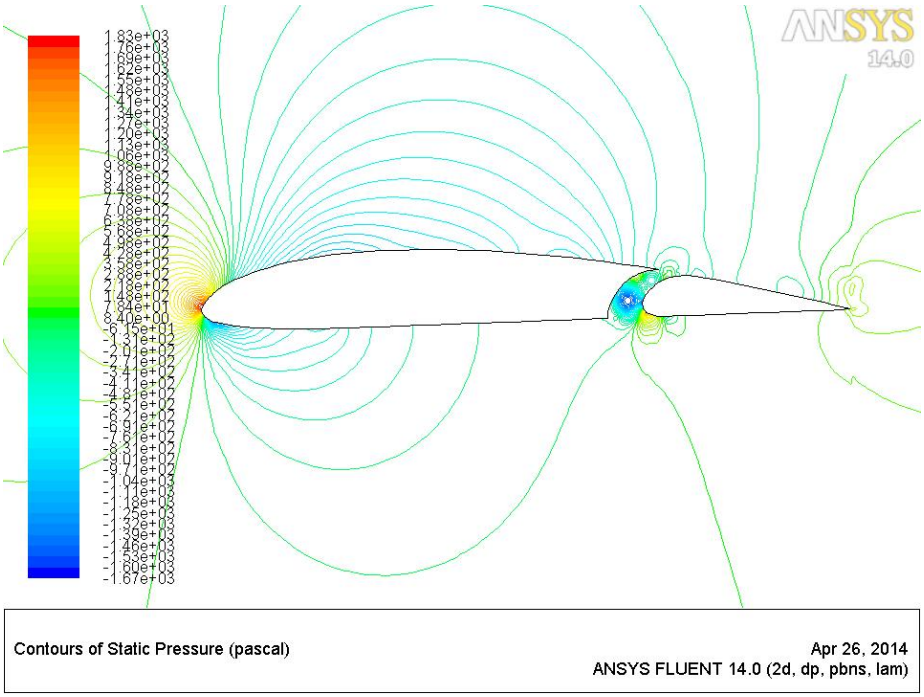

Figure 3.8: pressure contours of Clark Y aerofoil.

Observation is made that there is a low pressure zone created inside the slot as there are vortices formed inside it (see fig. 3.8). Also high pressure zone at the stagnation is observed, aerofoil as can be seen from the figure has two high pressure stagnation zones one at the leading edge of the main element one at leading edge of the flap. As observed from the contours the lower side pressure of both the main element and flap is higher than upper side pressure hence the aerofoil shows lifting capabilities.

Observation of velocity vectors is made and it is observed that a maximum velocity of 74 m/sec and minimum flow velocity approximately zero flow over the aerofoil (see fig. 3.9). Aerofoil shows smooth laminar flow and vortices are observed in the slot region. also a small trailing edge vortex is observed at the trailing edge of the flap. Vortices observed in the slot are shown in the fig. 3.9.

Separation and wake region behind the flow is observed using velocity contours as shown in fig. 3.11.

Figure 3.11 shows the wake region being formed behind the aerofoil. Also separation point can be observed on the flap surface. For precisely getting the

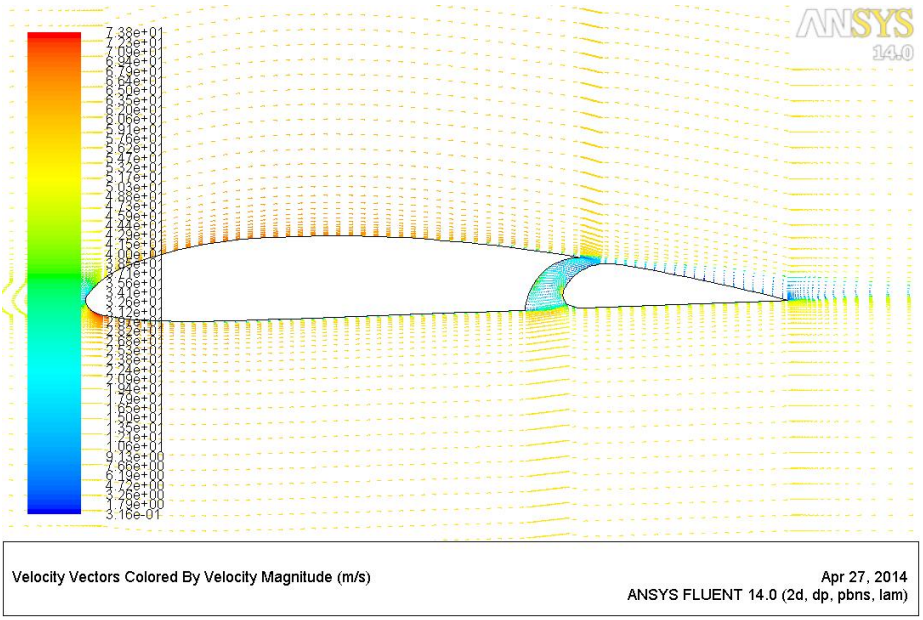

Figure 3.9: velocity vectors of Clark Y with no VG.

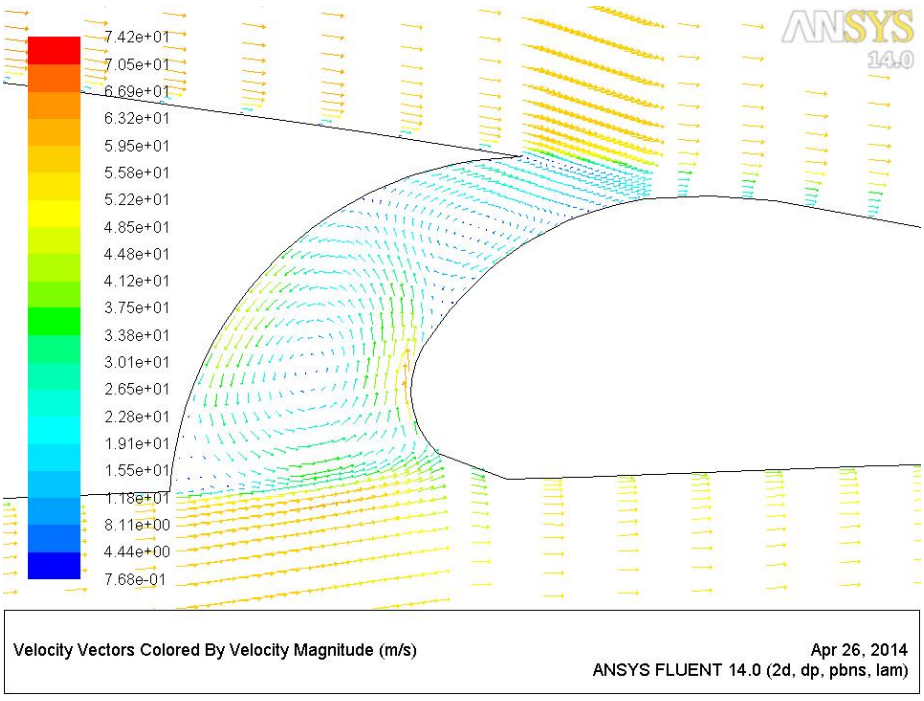

Figure 3.10: vortices inside the slot of Clark Y.

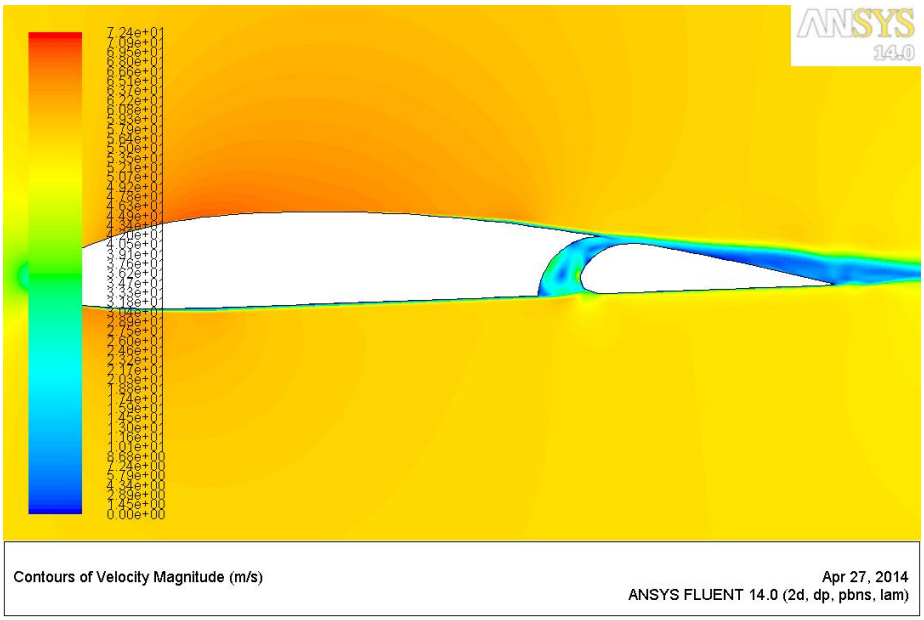

Figure 3.11: separation and wake developed in the aerofoil.

value of separation point C_f is plotted for the flap surface. As shown in fig. 3.12 C_f plot shows dropping of C_f to zero that exist due to separation of the flow. The results obtained are validated for C_L vs. α graph as shown in appendix D.

As C_f value tends to zero at 3.8 m location hence the location is the separation point of the aerofoil. The lower flap portion shows not much fluctuation in C_f as the flow is separation and wake free hence such profile exists.

To delay this separation and to enhance the aerodynamic performance of the flap various configurations of MVG's at various locations were tested following were some of locations at which CFD analysis was performed. These different locations are presented in fig. 3.13.

MVG's were place inside the slot MVG's used were triangular kind as shown in figure with dimensions of 2 mm wide and 2 mm high. Not much change was observed in the flow field characteristics. The configuration was tested for 2 to 10 MVG's placed in series but none showed positive results. The location of such VG's was varied from placing VG's on the slot to the upper surface of flap but no enhancement of aerodynamic characteristics were shown.

Single wishbone VG 6 mm wide and 2 mm high was used within the flap slot but not much changes were observed with such VG configuration. Also wishbone VG was used over the flap upper surface it showed some minor changes in enhancing the characteristics. Within the slot 2 to 5 wishbone VG's were tested at multiple locations but each case didn't show much of change from the original case.

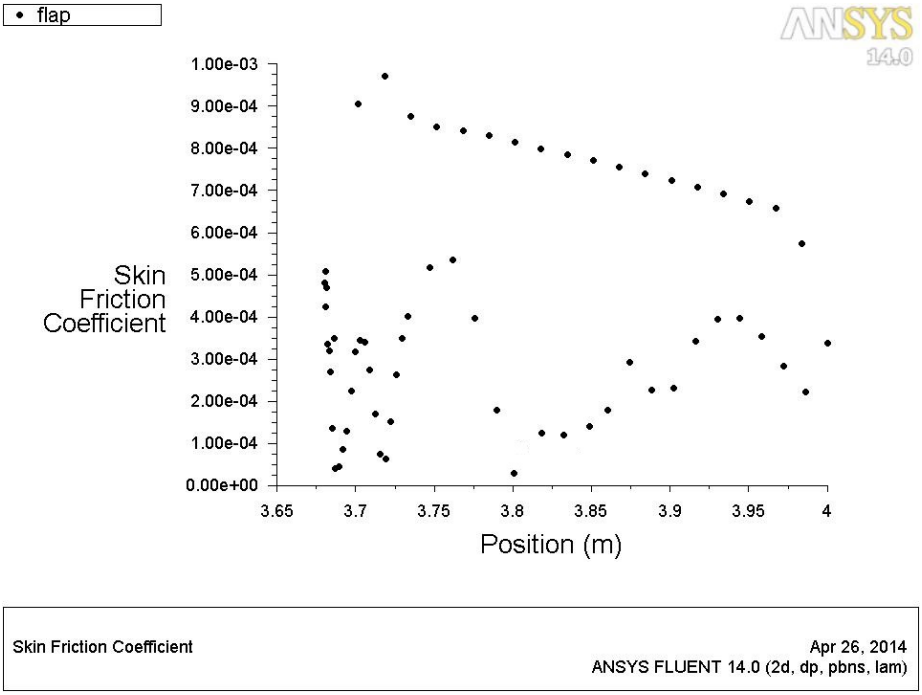

Figure 3.12: friction coefficient vs. position.

Wishbone MVG's were placed over the upper surface of the flap, 1 to 6 MVG configuration were tested 3 MVG's over the surface at about 25% flap chord showed improvement in the flow characteristics and the results are discussed below.

Using 3 wishbone MVG's over the flap surface proved that the separation point could be delayed as is shown in fig. 3.14.

As can be seen from fig. 3.14 the separation point before VG was 3.8 and after VG it is about 3.83, so the separation is delayed by almost 3 cm. The data file of this plot from fig. 3.14 is given appendix B.1. A FORTRAN code was developed in order to process and compare the C_f data. The details of working of this code is provided via a flowchart presented in appendix B.2. The full code itself is provided in appendix B.3. The results obtained by this code are summarized in table 3.5.

As can be observed form the table provided that C_f value has incensed by Adding the MVG's But separation point has shown a delay of 3 cm on the flap surface also there is a decrease in C_f on the lower flap surface but there is increase in the upper surface overall there is increase in C_f which is nearly 1% of the original C_f. As the separation is delayed this gives better aerodynamics of the flap hence enhancing its performance.

Coefficient of pressure C_p plots of with and without MVG's are shown in

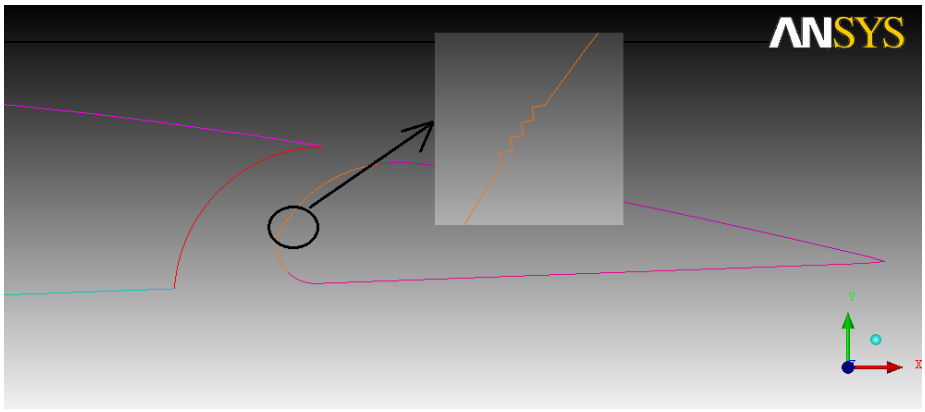

(a) configuration 1.

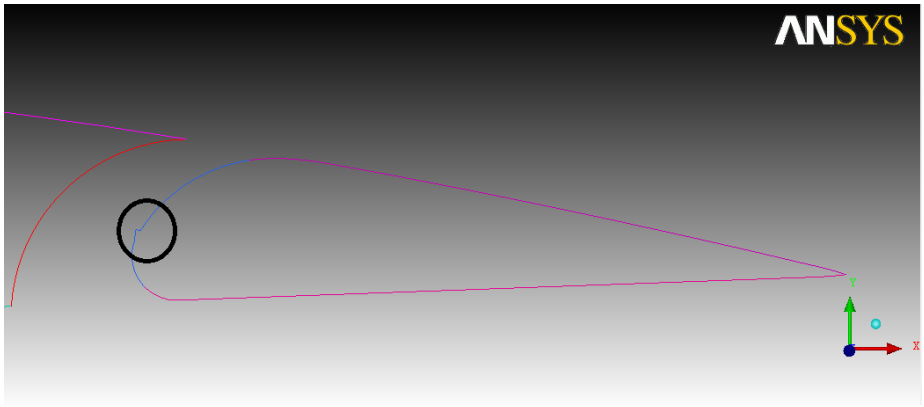

(b) configuration 2.

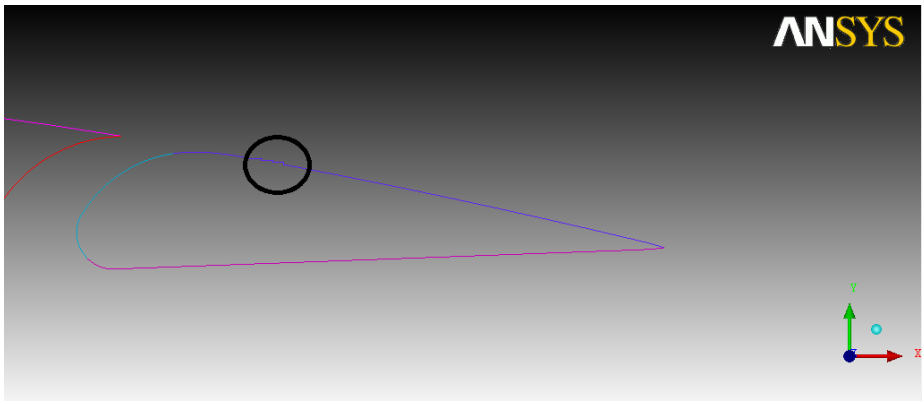

(c) configuration 3.

Figure 3.13: chosen positions of VG's on the flap.

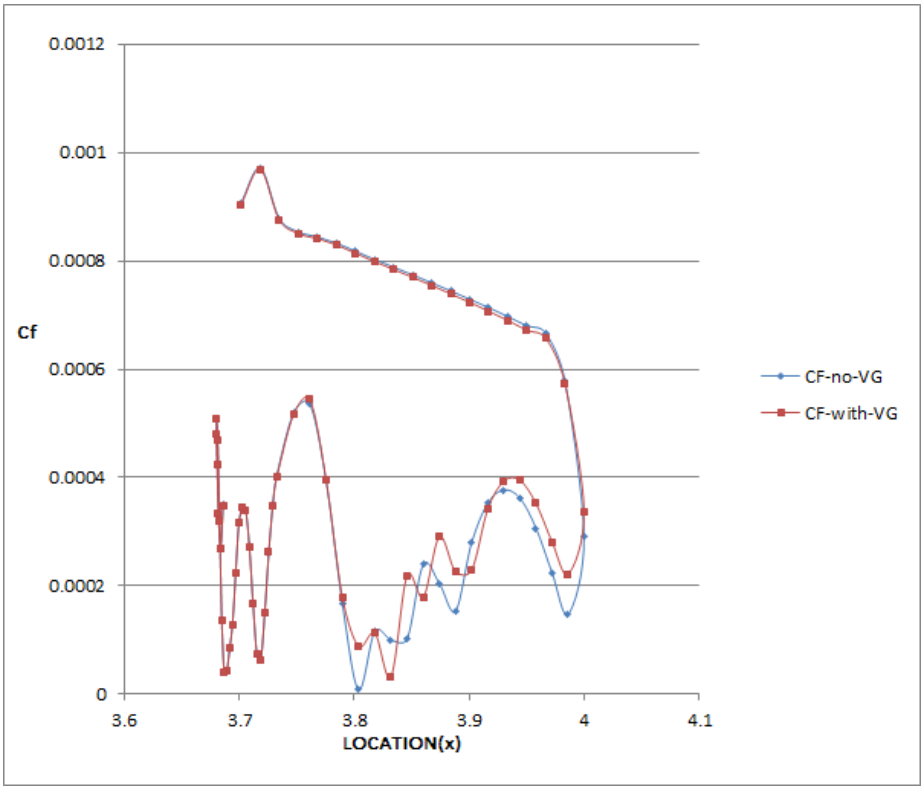

Figure 3.14: friction coefficient C_f comparison.

fig. 3.15. Data pertaining these plots are given in appendices C.1 to C.4. A FORTRAN code is developed to read the C_p values and find out lift and the drag developed by the flap and hence compare the values. The flowchart explaining the algorithm of the code is given in appendix C.5. The concerned FORTRAN codes also given in appendices C.6 and C.7.

Results obtained from the FORTRAN code are given in table 3.6. Coefficient of lift C_L can be obtained from coefficient of pressure C_p by using the following formula:

$$C_l = \frac{1}{c}\int_{LE}^{TE} C_{pl}(x)dx - \frac{1}{c}\int_{LE}^{TE} C_{pu}(x)dx \tag{3.11}$$

where c is the flap cord length, TE and LE are trailing and leading edge x coordinates, C_{pl} is the lower lift coefficient, and C_{pu} is the upper lift coefficient.

The FORTRAN code is run for the flap coordinates given table 3.7. The FORTRAN code then inputs the C_p values finds out the C_L values of the flap for the case with MVG's and without MVG's.

Hence, from the results in table 3.7 we see that there is about 25% increase in lift of flap of aerofoil flap when compared with the overall lift of the aerofoil 13% increase in lift was observed for the case with MVG's.

Table 3.5: C_f comparison.

Parameter	Value
No MVG'S	
C_f on lower flap surface	7.543190×10^{-4}
C_f on upper flap surface	2.591608×10^{-4}
With MVG'S	
C_f on lower flap surface	7.521700×10^{-1}
C_f on upper flap surface	2.682863×10^{-4}
Summary	
Increase in overall skin friction	6.976887×10^{-6}
Percentage increase in C_f	0.6884%

Table 3.6: C_L comparison ANSYS and FORTRAN results.

Solver	C_L value
ANSYS FLUENT	
Flap without MVG	0.1146200
Flap with MVG	0.1531900
FORTRAN Code	
Flap without MVG	0.1110461
Flap with MVG	0.1406270

Table 3.7: flap coordinates for Clark Y.

Parameter	Value
Flap LE	$3.68(x)$
Flap TE	$4(x)$
Flap Chord length	0.301

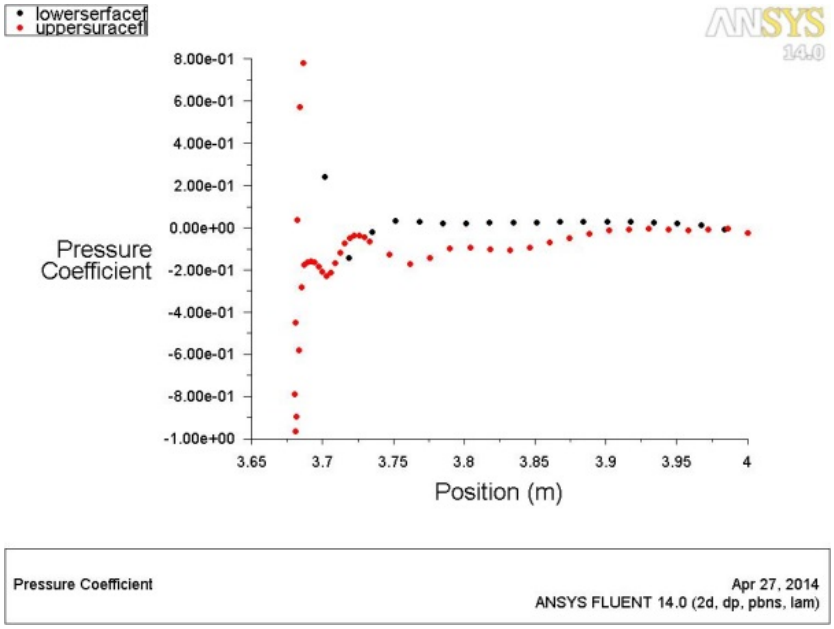

(a) C_p plot of flap without VG

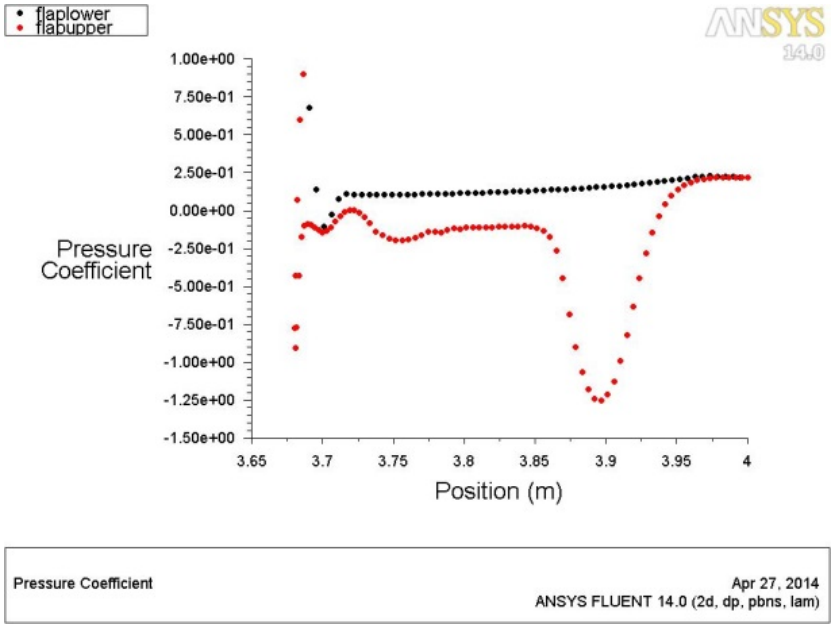

(b) C_p plot of flap with VG

Figure 3.15: Change in C_p due to VG.

Table 3.8: Aerodynamics of the Clark Y flap.

Flap	Coefficient of lift	Coefficient of drag	Aerodynamic efficiency
-	C_L	C_D	η
No MVG	0.11462	0.03150	3.6387
With MVG	0.15319	0.03617	4.2352

Finally, from table 3.8 observation can be made that although drag of the aerofoil is increased by 15% but there is overall increase in efficiency of the flap due to increase in C_L of the flap. hence from the discussion we conclude that careful placement of MVG's over the flap surface will lead to enhancement of aerodynamic performance of the flap.

3.9 Conclusion and recommendation

In this thesis discussion of various types and configurations of MVG's used with flap was made. It was concluded that configuration 3 in which series of Wishbone MVG's were placed together on the flap upper surface was the best location of such type of MVG's, it lead to enhancement of flap lift by almost 25% although drag over the flap was increased by 15% but overall the aerodynamic efficiency of the flap got increased.

On closing note it should be noted that not only do low profile VG's provide boundary layer control and flow separation control, but also it provides practical advantages of low installation cost, simplicity and low device drag these characteristics should be taken into account for its wide range of applications. Although MVG's may not replace the use of conventional VG's in all type of flow cases but may be used as a logical complement for some particular situations, such as cases where the separation region is fixed, MVG's may be placed close to the region hence improving on its flow conditions.

Appendix A

Clark Y aerofoil

A.1 Clark Y coordinates

x	y	x	y	x	y
1.37680	0.000824	0.362870	0.158130	0.24707	0.00195
1.36320	0.004566	0.335290	0.157370	0.27461	0.00238
1.34950	0.008299	0.307690	0.156010	0.30215	0.00262
1.33590	0.012019	0.280060	0.153910	0.32970	0.00272
1.32220	0.015713	0.252410	0.150950	0.35725	0.00272
1.29490	0.023005	0.224720	0.147100	0.38481	0.00265
1.26760	0.030147	0.197000	0.142370	0.41236	0.00256
1.24030	0.037143	0.169250	0.136700	0.43992	0.00249
1.21300	0.044003	0.141460	0.129930	0.46747	0.00244
1.18570	0.050722	0.113630	0.121850	0.49503	0.00239
1.15840	0.057297	0.085739	0.112250	0.52258	0.00235
1.13110	0.063720	0.071764	0.106570	0.55014	0.00231
1.10370	0.069993	0.057757	0.099966	0.57769	0.00227
1.07640	0.076105	0.043704	0.092045	0.60524	0.00222
1.04900	0.082060	0.029577	0.082002	0.63280	0.00217
1.02170	0.087850	0.018208	0.072045	0.66035	0.00212
0.99433	0.093480	0.012506	0.066564	0.68791	0.00207
0.96696	0.098944	0.006771	0.060137	0.71546	0.00201
0.93960	0.104240	0.003870	0.055938	0.74302	0.00196
0.91222	0.109360	0.002394	0.053130	0.77057	0.00192
0.88484	0.114280	0.001639	0.051244	0.79813	0.00187
0.85745	0.118990	0.000839	0.048050	0.82568	0.00182
0.83006	0.123470	0.000839	0.048050	0.85324	0.00177
0.80265	0.127710	0.001302	0.041600	0.88079	0.00172
0.77524	0.131700	0.001929	0.039826	0.90834	0.00167
0.74782	0.135440	0.003215	0.037206	0.93590	0.00162
0.72039	0.138940	0.005837	0.033392	0.96345	0.00157
0.69295	0.142190	0.011160	0.028008	0.99101	0.00152
0.66550	0.145190	0.016535	0.024119	1.01860	0.00147
0.63804	0.147920	0.027384	0.019195	1.04610	0.00142
0.61057	0.150360	0.041031	0.015503	1.07370	0.00137
0.58309	0.152480	0.054699	0.012388	1.10120	0.00132
0.55560	0.154280	0.068385	0.009810	1.12880	0.00127
0.52810	0.155720	0.082093	0.007840	1.15630	0.00122
0.50059	0.156830	0.109550	0.005047	1.18390	0.00117
0.47306	0.157620	0.137020	0.002820	1.21140	0.00112
0.44553	0.158140	0.164510	0.001056	1.23900	0.00107
0.41798	0.158410	0.192020	-0.00029	1.26660	0.00102
0.39043	0.158430	0.219540	-0.00127	1.29410	0.00097
0.36287	0.158130	0.247070	-0.00195	1.32170	0.00092

A.2 xy plot of points

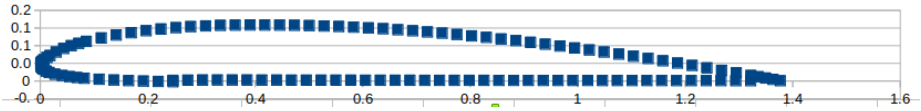

Figure A.1: Clark Y points.

Appendix B

Coefficient of friction

B.1 C_f with and without MVG of flap

Location x	Coefficient of friction with no VG C_f	Coefficient of friction with VG C_f
3.70158	0.0009070	0.000904359
3.71818	0.0009720	0.000969418
3.73476	0.0008790	0.000875989
3.75134	0.0008540	0.000850573
3.76792	0.0008440	0.000841087
3.78450	0.0008330	0.000829449
3.80108	0.0008180	0.000814206
3.81766	0.0008030	0.000798739
3.83424	0.0007890	0.000784323
3.85082	0.0007740	0.000769686
3.86740	0.0007600	0.000754615
3.88398	0.0007450	0.000739227
3.90056	0.0007290	0.000723446
3.91714	0.0007140	0.000706993
3.93371	0.0006970	0.000690042
3.95029	0.0006800	0.000671814
3.96687	0.0006660	0.000656664
3.98345	0.0005780	0.000573386
4.00000	0.0002910	0.000337213
3.98618	0.0001470	0.000220863
3.97222	0.0002240	0.000280992
3.95825	0.0003060	0.000351928
3.94426	0.0003620	0.000395061
3.93027	0.0003770	0.000393234
3.91626	0.0003530	0.000341435
3.90224	0.0002800	0.000228785
3.88822	0.0001540	0.000225806
3.87418	0.0002040	0.000290871
3.86014	0.0002390	0.000178724
3.84608	0.0001010	0.000219000
3.83201	0.0001000	0.000031800
3.81793	0.0001160	0.000112843
3.80385	0.0000080	0.000088400
3.78974	0.0001680	0.000178719
3.77563	0.0003940	0.000394991
3.76149	0.0005350	0.000543908
3.74719	0.0005190	0.000515952
3.73286	0.0004050	0.000401018
3.72925	0.0003510	0.000348933
3.72569	0.0002610	0.000262411
3.72217	0.0001500	0.000150767
3.71870	0.0000613	0.000062400
3.71531	0.0000745	0.000074000
3.71199	0.0001710	0.000167886
3.70877	0.0002740	0.000272514
3.70562	0.0003390	0.000338626
3.70258	0.0003440	0.000344128
3.69965	0.0003150	0.000315492
3.69685	0.0002220	0.000222234
3.69415	0.0001290	0.000128309
3.69158	0.0000837	0.000084000
3.68918	0.0000421	0.000042900
3.68696	0.0000404	0.000040000
3.68482	0.0001360	0.000135298
3.68279	0.0003200	0.000319367
3.68121	0.0004700	0.000468955
3.68033	0.0005090	0.000507659
3.68018	0.0004810	0.000479907
3.68074	0.0004240	0.000423578
3.68190	0.0003350	0.000334338
3.68369	0.0002700	0.000269546
3.68602	0.0003490	0.000348749

B.2 Flowchart to compare C_f

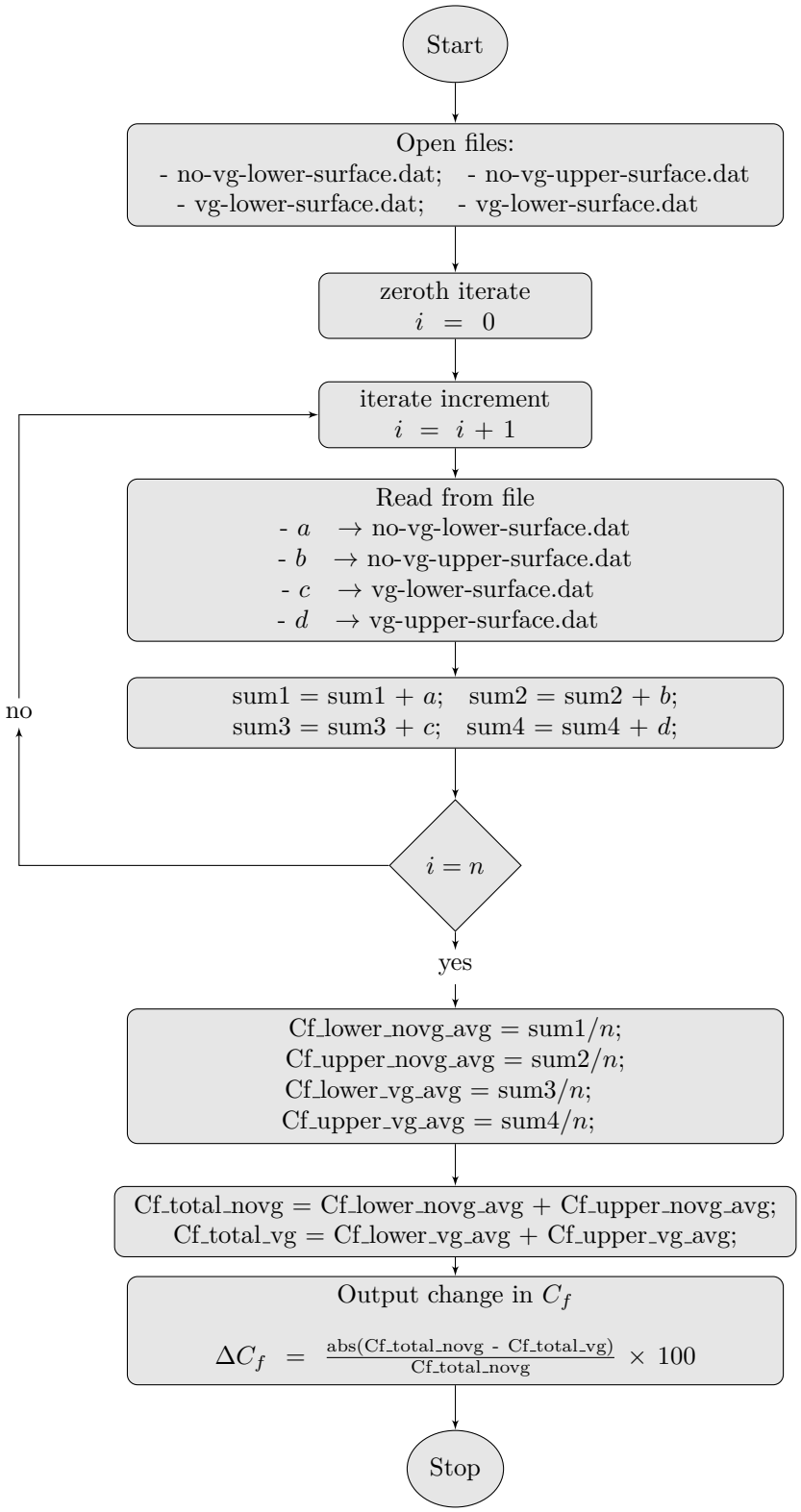

B.3 FORTRAN code to compare C_f

```
Program cf_compare
implicit none

!********* Variables used ********************
integer i,k
real cf,cf_Vg,sum1,sum2,n1,n2
real cflower1,cfupper1,cflower2,cfupper2
!*********************************************

!*********** Opening files that contain input data***********
open (unit=1, file="novglowersuface.dat")
open (unit=2, file="vglowersurface.dat")
open (unit=3, file="novguppersurface.dat")
open (unit=4, file="vguppersurface.dat")
!************************************************************

!******************upper surface Cf************************
do i=1,43  !do loop to read input of the upper surface

read(3,*) n1        !reading the input
read(4,*) n2        !reading the input
sum1= sum1+n1       !summing up the input for no VG case
sum2= sum2+n2       !summing up the input for  VG case
end do

cfupper1=sum1/43      !Average Cf on upper surface with No VG
cfupper2=sum2/43      !Average Cf on Upper Surface with VG
!************************************************************

sum1=0
sum2=0
n1=0
n2=2

!***************** Lower surface Cf************************
do i=1,19      !do loop to read input of lower surface

read(1,*) n1       !reading input from file 1
read(2,*) n2       !reading input from file 2
sum1= sum1+n1      !summing up the input for no VG case
sum2= sum2+n2      !summing up the input for VG case
end do
!*****************************************************

cflower1=sum1/19      !Average Cf on lower surface No VG
cflower2=sum2/19      !Average Cf on lower surface with VG

close(1)
close(2)
close(3)
close(4)

!******************printing results*****************
print*,"average lower surface cf NO VG:",cflower1
print*,"average lower surface cf WITH VG:",cflower2
print*,"average upper surface cf NO VG:",cfupper1
print*,"average upper surface cf WITH VG:",cfupper2

! claculating change in cf
cf = abs((cflower1+cfupper1) -(cflower2+cfupper2))
```

```
61
62 print*, "increase in skinfriction due to VG:",cf
63
64 !calculating %ange change in cf
65 cf_Vg= cf*100/(cflower1+cfupper1)
66
67 print*, "percentage increase in cf:", cf_Vg
68
69 read*,k
70 end program cf_compare
```

Appendix C

Coefficient of pressure & lift

C.1 C_p of lower surface with VG

location x	Coefficient of pressure C_p	location x	Coefficient of pressure C_p
3.70593	-0.02291	3.85566	0.132578
3.71128	0.078849	3.86101	0.134994
3.71662	0.107310	3.86635	0.137525
3.72197	0.104856	3.87170	0.140179
3.72732	0.101920	3.87705	0.142966
3.73267	0.100618	3.88240	0.145898
3.73801	0.100212	3.88774	0.148988
3.74336	0.100667	3.89309	0.152253
3.74871	0.101675	3.89844	0.155713
3.75406	0.102885	3.90379	0.159391
3.75940	0.104171	3.90913	0.163315
3.76475	0.105377	3.91448	0.167518
3.77010	0.106425	3.91983	0.172039
3.77545	0.107434	3.92518	0.176917
3.78079	0.108507	3.93052	0.182188
3.78614	0.109671	3.93587	0.187900
3.79149	0.110923	3.94122	0.194113
3.79684	0.112259	3.94657	0.200763
3.80218	0.113675	3.95191	0.207671
3.80753	0.115172	3.95726	0.214468
3.81288	0.116752	3.96261	0.220127
3.81823	0.118416	3.96796	0.223397
3.82357	0.120168	3.97330	0.223408
3.82892	0.122006	3.97865	0.222306
3.83427	0.123933	3.98400	0.220494
3.83962	0.125950	3.98934	0.220770
3.84496	0.128062	3.99468	0.218671
3.85031	0.130269	4.00000	0.218919

C.2 C_p of upper surface with VG

location x	Coefficient of pressure C_p	location x	Coefficient of pressure C_p
3.70258	-0.1410	3.84663	-0.10121
3.70562	0.11523	3.85117	-0.10968
3.70877	0.07867	3.85570	-0.12711
3.71199	0.04138	3.86023	-0.15984
3.71531	0.01345	3.86476	-0.23701
3.71870	0.00034	3.86928	-0.40572
3.72217	0.00135	3.87381	-0.64655
3.72569	0.01719	3.87833	-0.87771
3.72925	0.04469	3.88286	-1.05614
3.73286	-0.0865	3.88739	-1.18029
3.73746	0.13836	3.89191	-1.25054
3.74207	0.16493	3.89643	-1.26736
3.74670	0.18728	3.90095	-1.23408
3.75132	0.19973	3.90547	-1.15185
3.75593	0.20125	3.90999	-1.02199
3.76053	0.19386	3.91451	-0.85378
3.76511	0.18034	3.91903	-0.66587
3.76967	0.16283	3.92354	-0.47877
3.77423	0.14212	3.92806	-0.30911
3.77885	0.14155	3.93257	-0.16781
3.78335	0.14751	3.93708	-0.05738
3.78785	-0.1258	3.94159	0.025484
3.79247	0.11736	3.94610	0.085696
3.79670	0.11992	3.95061	0.128438
3.80124	0.11287	3.95512	0.158494
3.80579	-0.1108	3.95963	0.179627
3.81033	0.10917	3.96413	0.194367
3.81487	0.10828	3.96864	0.20433
3.81941	0.10738	3.97314	0.210648
3.82395	-0.1064	3.97764	0.214323
3.82849	0.10509	3.98215	0.216266
3.83303	0.10317	3.98665	0.217233
3.83756	-0.10084	3.99115	0.217671
3.84210	-0.09917	3.99560	0.217876
		4.00000	0.218919

C.3 C_p on lower surface with no VG

location x	Coefficient of pressure C_p
3.71818	-0.14627
3.73476	-0.02277
3.75134	0.030547
3.76792	0.025003
3.78450	0.018813
3.80108	0.019850
3.81766	0.022257
3.83424	0.023325
3.85082	0.024082
3.86740	0.025011
3.88398	0.025699
3.90056	0.025915
3.91714	0.025429
3.93371	0.023799
3.95029	0.019560
3.96687	0.010812
3.98345	-0.00901
4.00000	-0.02494

C.4 C_p on upper surface with no VG

location x	Coefficient of pressure C_p
3.69415	0.16705
3.69685	0.18361
3.69965	0.21155
3.70258	0.23093
3.70562	0.21536
3.70877	0.17082
3.71199	0.11875
3.71531	0.07511
3.7187	0.04909
3.72217	0.03894
3.72569	0.03956
3.72925	0.04774
3.73286	0.06601
3.74719	0.12862
3.76149	0.17244
3.77563	0.14354
3.78974	0.10066
3.80385	0.09369
3.81793	0.10242
3.83201	0.10707
3.84608	0.09572
3.86014	-0.0728
3.87418	0.04975
3.88822	0.03015
3.90224	0.01559
3.91626	0.00805
3.93027	0.00704
3.94426	0.01022
3.95825	0.01492
3.97222	0.01007
3.98618	0.00453
4.00000	0.02494

C.5 Flowchart to calculate C_L from C_p

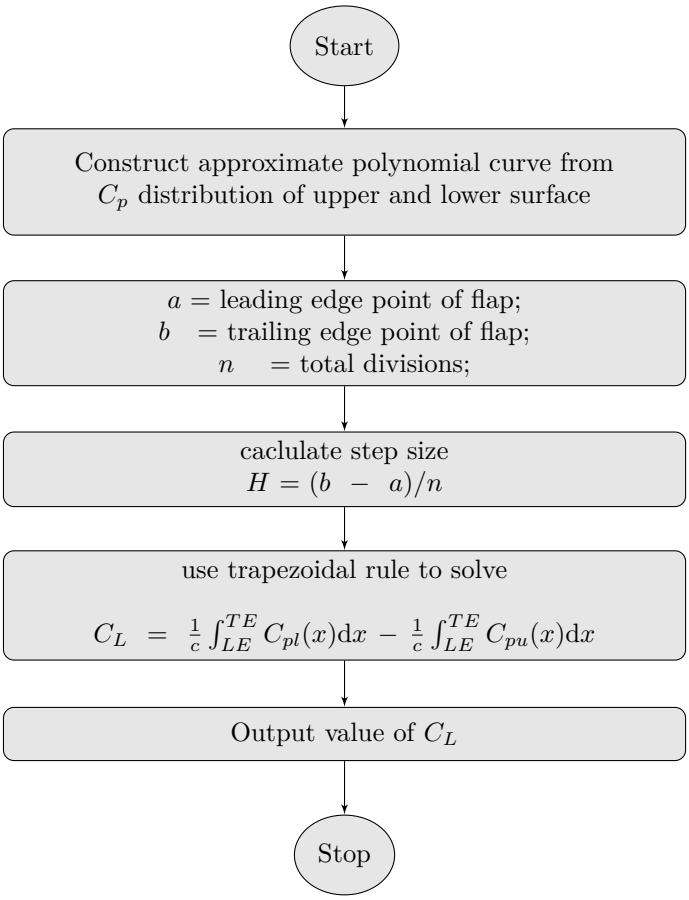

C.6 FORTRAN code to calculate C_L from C_p distribution given above for no MVG on aerofoil flap

```
program Cl_novg
implicit none

!*********** variables used************
real a,b,c,h,sl,su,fxcpl,fxcpu,x,y,sum,xi
integer i,j,k,n

print*, "enter the lower limit " !coordinates of flap LE
read*, a

print*, "enter the upper limit"    !coordinated of lap TE
read*, b

!trapizoidal rule total divisions
print*, "enter the total number of divisions"
read*, n
```

```
17
18 h  = (b-a)/n        !increment
19 sum = 0
20
21 do i= 1,n-1  !do loop calculating cp of lower integral formula
22 xi=a + (i*h)
23
24 sum = sum + fxcpl(xi)
25 end do
26
27 sl = (-h*0.5) * (fxcpl(a) + fxcpl(b) +(2*sum)) !cp lower surface
28 sum = 0
29
30 do i= 1,n-1 !do loop calculating cp on the upper surface
31 xi=a + (i*h)
32
33 sum = sum + fxcpu(xi)
34 end do
35
36 su = (-h*0.5) * (fxcpu(a) + fxcpu(b) +(2*sum)) !cp upper surface
37
38 print*, "cl of the flap is :",sl,su,(sl-su)/(30) !30 is c of flap
39 read*,k
40
41 end program CL_NOVG
42
43
44 !********************** fuction for lower surface***************
45 function fxcpl(x) result(y)
46 real  x,y
47
48 !fuction calculated using excel plotting
49 y=(-510.6*x**4)+(7907.9*x**3)-(45923*x**2)+(118509*x)-(114671)
50 end function fxcpl
51
52
53 !****************** function for upper surface******************
54 function fxcpu(x) result(y)
55 real  x,y
56
57 !calculated using excel
58 y=(-534.14*x**4)+(8217.3*x**3)-(47395*x**2)+(121465*x)-116707
59
60 end function fxcpu
```

C.7 FORTRAN code to calculate C_L from C_p distribution given above for MVG on aerofoil flap

```
1 program Cl_vg
2 implicit none
3
4 !*********** variables used************
5 real a,b,h,sl,su,fxcpl,fxcpu1,sum,xi,h1,su1,su2,h2,fxcpu2
6 integer i,k,n
7
8 print*, "enter the lower limit " !coordinaytes of flap LE
9 read*, a
10
11 print*, "enter the upper limit"    !coordinated of lap TE
```

```
read*, b

!trapizoidal rule total divisions
print*, "enter the total number of divisions"
read*, n

h  = (b-a)/n        !increment
sum = 0

do i= 1,n-1  !do loop calculating cp of lower integral formula
xi=a + (i*h)

sum = sum + fxcpl(xi)
end do

sl = (h*0.5) * (fxcpl(a) + fxcpl(b) +(2*sum)) !cp lower surface
sum = 0
h1= (3.85-3.7)/n

do i= 1,n-1   !do loop calculating cp on the upper surface
xi=3.7 + (i*h1)

sum = sum + fxcpu1(xi)
end do

!cp of upper surface
su1 = (h1*0.5) * (fxcpu1(3.7) + fxcpu1(3.85) +(2*sum))

sum = 0
h2 = (4-3.9)/n

do i= 1,n-1   !do loop calculating cp on the upper surface
xi=3.9 + (i*h2)

sum = sum + fxcpu2(xi)
end do

!cp of upper surface
su2 = (h1*0.5) * (fxcpu1(3.9) + fxcpu1(4) +(2*sum))

su= (su1+su2)

print*, "cl of the flap is :",sl,su,(su-sl)/(30)     !30 is c of
    flap
read*,k

end program CL_VG


!********************** fuction for lower surface***************
function fxcpl(x) result(y)
real  x,y

!fuction calculated using excel plotting
y=(-251.07*x**4) + (3876.9*x**3) - (22443*x**2) +(57729*x)-55671
end function fxcpl

!*********** function for upper surface (3.7 to 3.85)************
function fxcpu1(x) result(y)
real  x,y

!calculated using excel
```

```
73 y=(-738.17*x**3)+(8372.7*x**2)-(31778*x)+40200
74
75 end function fxcpu1
76
77 !*********** function for upper surface (3.85 to 4)**************
78 function fxcpu2(x) result(y)
79 real  x,y
80
81 !calculated using excel
82 y=(-6356.6*x**3)+(74953*x**2)-(294575*x)+(385867)
83
84 end function fxcpu2
```

Appendix D

Validation

Validation of results from ANSYS comparison with experimental results with research paper from Fred E. Whick, Joseph A Shortal, Multiple fixed Slots and A Trailing Edge Flap on the lift and drag of Clark Y airfoil. NACA report 427 [19].

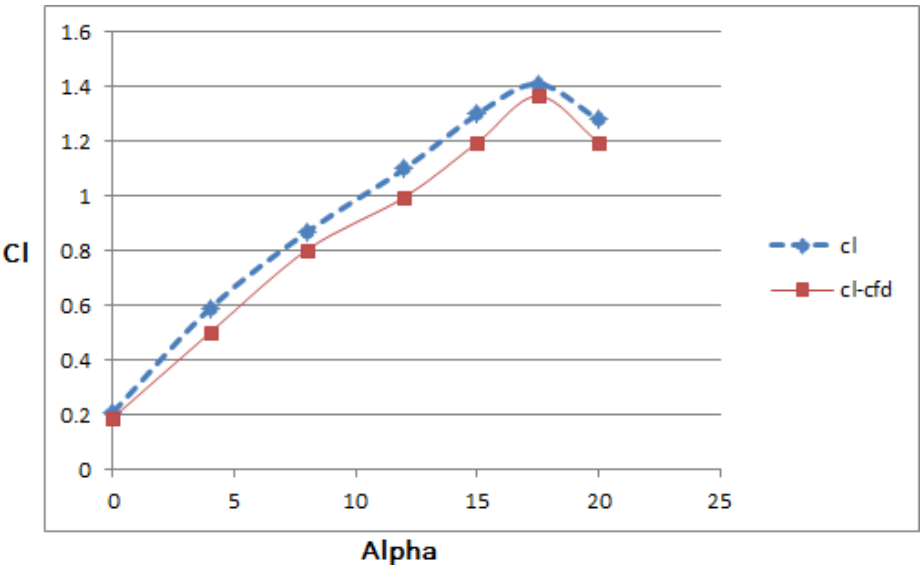

Figure D.1: Clark Y points.

Maximum error of 12.3% is observed when compared with experimental results.

Table D.1: ANSYS FLUENT results for Clark Y without vortex generators.

Angle of attack α	Coefficient of lift C_L
0.0	0.18970
4.0	0.50123
8.0	0.80411
12.0	0.99632
15.0	1.19610
17.5	1.36650
20.0	1.19651

Bibliography

[1] Harold D Taylor. The elimination of diffuser separation by vortex generators. *Research department report no. r-4012-3, United Aircraft Corporation, East Hartford, Connecticut*, 103, 1947.

[2] Galen Brandt Schubauer and WG Spangenberg. Forced mixing in boundary layers. *Journal of Fluid Mechanics*, 8(1):10–32, 1960.

[3] Bruce L Storms and Cory S Jang. Lift enhancement of an airfoil using a gurney flap and vortex generators. *Journal of Aircraft*, 31(3):542–547, 1994.

[4] MJ Werle, RW Paterson, and WM Presz Jr. Trailing-edge separation/stall alleviation. *AIAA journal*, 25(4):624–626, 1987.

[5] Hua Shan, Li Jiang, Chaoqun Liu, Michael Love, and Brant Maines. Numerical study of passive and active flow separation control over a NACA0012 airfoil. *Computers & fluids*, 37(8):975–992, 2008.

[6] John C Lin. Review of research on low-profile vortex generators to control boundary-layer separation. *Progress in Aerospace Sciences*, 38(4-5):389–420, 2002.

[7] Gilles Godard, Jean-Marc Foucaut, and Michel Stanislas. Control of a decelerating boundary layer. part 2: Optimization of slotted jets vortex generators. *Aerospace Science and Technology*, 10(5):394–400, 2006.

[8] Takaaki Shizawa and Yoshiyuki Mizusaki. Response of time-depended flowfield structure behind an active vortex generators pair. In *42nd AIAA Aerospace Sciences Meeting and Exhibit*, page 427, 2004.

[9] M Kerho, S Hutcherson, RF Blackwelder, and RH Liebeck. Vortex generators used to control laminar separation bubbles. *Journal of aircraft*, 30(3): 315–319, 1993.

[10] NASA. Micro-vortex generators enhance aircraft performance. URL `https://www.nasa.gov/centers/langley/news/factsheets/Micro-VG.html`.

[11] John C Lin, Stephen K Robinson, Robert J McGhee, and Walter O Valarezo. Separation control on high-lift airfoils via micro-vortex generators. *Journal of aircraft*, 31(6):1317–1323, 1994.

[12] P Ashill, J Fulker, and K Hackett. Research at dera on sub boundary layer vortex generators (sbvgs). In *39th aerospace sciences meeting and exhibit*, page 887, 2001.

[13] PR Ashill and GL Riddle. Control of leading-edge separation on a cambered delta wing. In *AGARD CONFERENCE PROCEEDINGS AGARD CP*, pages 11–11. AGARD, 1994.

[14] Kevin Langan and Jeffrey Samuels. Experimental investigation of maneuver performance enhancements on an advanced fighter/attack aircraft. In *33rd Aerospace Sciences Meeting and Exhibit*, page 442, 1995.

[15] Frank K Lu, Qin Li, and Chaoqun Liu. Microvortex generators in high-speed flow. *Progress in Aerospace Sciences*, 53:30–45, 2012.

[16] P Ashill, J Fulker, and K Hackett. Studies of flows induced by sub boundary layer vortex generators (sbvgs). In *40th AIAA aerospace sciences meeting & exhibit*, page 968, 2002.

[17] John David Anderson Jr. *Fundamentals of aerodynamics*. Tata McGraw-Hill Education, 2010.

[18] HK Versteeg and W Malalasekera. Computational fluid dynamics. *The finite volume method*, 1995.

[19] Fred E Weick and Joseph A Shortal. The effect of multiple fixed slots and a trailing-edge flap on the lift and drag of a clark y airfoil. *NACA report 427*, 1933.